

Research Article

Research on Stability Control Technology of Mining Roadway Based on Energy Transformation

Guohua Zhang , Yanwei Duan , and Tao Qin 

Key Laboratory of Mining Engineering of Heilongjiang Province College, Heilongjiang University of Science and Technology, Harbin 150022, China

Correspondence should be addressed to Yanwei Duan; 1354070597@qq.com

Received 26 November 2021; Revised 22 April 2022; Accepted 13 June 2022; Published 19 January 2023

Academic Editor: Zhijie Wen

Copyright © 2023 Guohua Zhang et al. This is an open access article distributed under the Creative Commons Attribution License, which permits unrestricted use, distribution, and reproduction in any medium, provided the original work is properly cited.

The process of roadway surrounding rock deformation and instability is always accompanied by energy changes, and the energy transformation of surrounding rock directly drives its deformation and failure. In order to realize the stability control of mining roadway, the distribution of elastic strain energy and plastic strain energy of surrounding rock was analyzed by using FLAC^{3D} numerical simulation software on the basis of the energy transformation law of sandstone under different confining pressures revealed by indoor triaxial compression test. Based on this, combined with the energy transformation, the principle of roadway surrounding rock stability control technology is proposed. One is to reduce the elastic strain energy of surrounding rock, that is, by increasing the extension of support body, part of the roadway energy is transferred to the support body, so as to improve the energy release of surrounding rock, or by optimizing the layout of roadway to reduce the energy accumulation of surrounding rock. The second is to increase the plastic strain energy of surrounding rock, that is, to increase the energy dissipation of surrounding rock by setting weak structure. The above research results are applied to the surrounding rock control of the right second transport roadway in the 91st coal of Xinjian coal mine. After the optimization of support measures, the roadway surface displacement and its increase rate decreased significantly, roof subsidence decreased from 247 mm to 62 mm, floor heave decreased from 120 mm to 26 mm, and the right rib shrinkage decreased from 292 mm to 94 mm, that is, the floor heave control effect was particularly obvious. The deformation of surrounding rock gradually stabilized after 45 days.

1. Introduction

The rapid development of China's economy is inseparable from energy. Coal accounts for about 70% of the primary energy consumption structure. Therefore, the safe production of coal mines is of great significance to economic development [1–3]. In coal mine safety accidents, the accidents caused by deformation and instability of surrounding rock account for a large proportion [3]. Ensuring the stability of surrounding rock is the premise of coal mine production. In the study of surrounding rock stability, scholars often analyzed the surrounding rock stability from the perspective of mechanics, but the complex geological conditions (large buried depth, faults, soft rock, etc.) often made the mechanical analysis process become complicated [4–8]. In fact, the

deformation and failure process of surrounding rock is a process with energy changes from local deformation to overall damage and finally failure. Due to energy accumulation caused by roadway excavation, the energy may be higher than its energy storage limit, which causes deformation of the surrounding rock, and this part of energy will be released concentratedly, resulting in the failure of the surrounding rock. Energy change is the external performance of material physical change, and the great change will cause material damage. Therefore, energy transformation directly drives deformation and failure of surrounding rock, from the perspective of energy interpretation of surrounding rock can reflect its essence [9–11].

For the study of surrounding rock stability related to energy, scholars have done a lot of research from laboratory

experiments and numerical simulation. On the one hand, laboratory experiments are mainly conducted to explore the characteristics and laws of rock energy evolution through rock mechanics experiments under different stress paths. From the perspective of energy, Xu et al. [12] analyzed the deformation and damage process of sandstone under the action of circulating pore water pressure, and discussed the evolution law of energy absorption and release in this process. Zhao et al. [13] carried out three confining pressure unloading tests under different unloading paths to study the energy evolution characteristics and evolution rate of rock under unloading conditions. By carrying out triaxial cyclic loading and unloading experiments, Yang et al. [14] discussed the energy evolution characteristics of postpeak stress drop stage and postpeak residual stress stage. Liu et al. [15] studied the energy evolution law and linear storage law of red sandstone in the creep process by conducting uniaxial graded creep test and uniaxial cyclic loading and unloading test after creep. Meng et al. [16] carried out triaxial cyclic loading and unloading tests of limestone under six kinds of confining pressures, revealing the confining pressure effect of energy evolution process and distribution law of loaded rock samples.

On the other hand, the numerical simulation mainly carries out the energy characteristics of surrounding rock under different working conditions. Hao et al. [17] used FLAC^{3D} to simulate the advance process of working face, analyzed the morphological characteristics and energy distribution characteristics of roadway plastic area within 100 m of the front working face when the advance was 400 m, and revealed the relationship between the morphological distribution and energy of roadway plastic area. By using discrete element simulation software PFC, Yu et al. [18] analyzed the energy and dynamic acoustic emission evolution law of roadway excavation, and discussed the influence of different vertical stresses and lateral pressure coefficients on roadway excavation energy evolution. Shi et al. [19] used FLAC^{3D} to simulate the process of working face, analyzed the energy evolution and release law of surrounding rock in stope, and pointed out that the roof and the front of coal wall were the key areas of energy accumulation or release. Wang et al. [20] used FLAC^{3D} simulation software to analyze the evolution law of elastic energy of the roof, two ribs and driving face under different driving speeds, which was used as the basis for establishing the evolution mechanism of rock burst energy zoning. Huang et al. [21] used FLAC^{3D} to simulate the stress distribution before and after filling gangue in goaf, and then obtained the distribution of elastic strain energy before and after filling. Ma et al. [22] used UDEC to analyze the energy evolution law of roadway surrounding rock under roof of different thickness, and optimized roadway support parameters according to the simulation results, effectively solving the problem of large deformation of roadway.

Based on the analysis of the above studies, the study of surrounding rock stability related to energy mainly focuses on the laboratory study of rock energy evolution law and the numerical simulation study of surrounding rock energy characteristics, while the study of roadway surrounding rock

stability control based on energy characteristics is relatively insufficient. In this paper, the mining roadway of Xinjian coal mine is taken as the engineering background. Triaxial compression tests were carried out in the laboratory to reveal the energy evolution law of sandstone under different confining pressures. FLAC^{3D} numerical simulation software was used to analyze the distribution law of elastic strain energy and plastic strain energy of roadway surrounding rock. Based on this, combined with the energy transformation, the principle of roadway surrounding rock stability control technology is proposed. The monitoring results showed that the roadway surface displacement and its increasing speed decreased obviously after the optimization of support measures, which effectively solved the roadway control problem and provided reference for roadway surrounding rock stability control under similar conditions.

2. Energy Evolution Characteristics of Rock Deformation and Failure Process

2.1. Test Scheme. In order to obtain the characteristics of energy evolution during the deformation and failure of the rock specimens, the conventional triaxial loading test was conducted on the sandstone samples from Xinjian Coal Mine in Qitaihe in China with TOP INDUSTRIE Rock 600-50 automatic servo rock rheometer (see Figure 1). The rock specimen was a standard cylinder (50 mm in diameter and 100 mm in height). Axial pressure was applied at a rate of 0.1 mm/min and confining pressure was applied at a rate of 0.05 MPa/s. The predetermined confining pressure was 5 MPa, 10 MPa, 15 MPa, and 20 MPa.

2.2. Energy Calculation Method Based on Test Data. The loading process of the rock specimens is always accompanied by the storage and dissipation of energy. Both of the variables representing the energy storage and dissipation inside rock are elastic energy and dissipated energy. In the experiment, these two variables cannot be recorded in real time. Therefore, they are calculated through stress-strain curves that are easily accessible. Figure 2 shows the calculation method. The shaded area denotes the elastic strain energy (U^e) stored by the deformation of the rock specimens, and E^u denotes the unloading modulus of the rock specimens. The dissipated energy (U^d) is the area constrained by the unloading modulus, the stress-strain curve and the horizontal axis.

According to the first law of thermodynamics, supposing the experiment system is a closed system ignoring the thermal energy dissipation in the experiment, the total energy U generated by the work done by external force is [23–27]

$$U = U^e + U^d = \int \sigma_1 d\varepsilon_1 = \sum_{i=0}^n \frac{1}{2} (\varepsilon_{1i+1} - \varepsilon_{1i}) (\sigma_{1i} + \sigma_{1i+1}), \quad (1)$$

where U^e is elastic strain energy, U^d is dissipated energy and σ_{1i} , ε_{1i} , σ_{3i} , and ε_{3i} are axial stress, axial strain, circumferential stress, and circumferential strain, respectively.



FIGURE 1: TOP INDUSTRIE Rock 600-50 automatic servo rock rheometer.

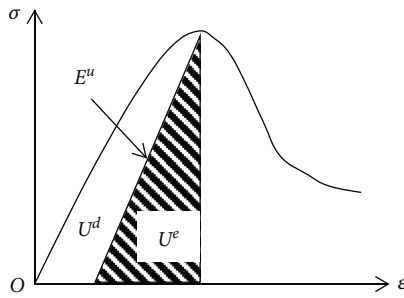


FIGURE 2: Energy calculation method.

The expression of triaxial compression elastic energy is

$$U^e = \frac{1}{2E_u} [\sigma_1^2 + 2\sigma_3^2 - 2\mu(2\sigma_1\sigma_3 + \sigma_2\sigma_3)], \quad (2)$$

where E_u is unloading modulus and μ is about 50%~60% of the peak strength [28–30].

2.3. Characteristic Law of Rock Energy Evolution. It is assumed that the loading system is a closed system with no heat exchange with the external environment. In the loading system, external load input mechanical energy is absorbed by rock specimens, the rock specimens elastic deformation occur in the form of elastic strain energy stored within rock specimens. As the load goes on, the elastic strain energy stored by the rock specimens become less and less, and the energy absorbed at this time is mainly used to produce microcracks inside the rock specimens, namely, the part of energy is dissipated. In order to compare and analyze the law of energy evolution corresponding to different stages of stress-strain curves, axial strain is used as the horizontal axis, axial stress as the left axis, and energy density as the right axis. The energy evolution curves of the conventional triaxial compression test sandstone under different confining pressures are shown in Figure 3.

It can be seen that the energy evolution process can be divided into prepeak stage and postpeak stage according to

the stress-strain curve in Figure 3 and that different energy evolution curves under different confining pressures have similar characteristics.

- (1) As axial strain increases, total energy U increased exponentially before the axial stress peak and the growth rate decreased slightly after the stress peak. The growth rate is correlated with the properties of stress and strain. The maximum of U varied under different confining pressures. It increased with the increase of confining pressure
- (2) Elastic strain energy U^e indicates the releasable energy stored in the rock specimens, the evolution law is consistent with the stress-strain curve. In the prepeak stage, the difference between U^e and U was not great. After reaching the peak, U^e dropped rapidly. Also, the difference increased as the axial strain increased. The law of U^e is consistent with the stress-strain curve, which is positively associated with the confining pressure
- (3) Dissipated energy U^d indicates the energy consumed by the rock specimens during plastic deformation, crack expansion and energy release, which is irreversible. The evolution trend of U^d was slow growth before the peak but rapid growth after the peak. It grew almost exponentially and quickly became a major component of energy. The maximum of U^d varied under different confining pressures and increased with the increase in confining pressure. After the peak, the growth rate of U^d also increased slightly with the increase in confining pressure

To study the transformation of the energy in different stages, the corresponding energy characteristics of each stage are drawn in the bar graphs, and Figure 4 shows the energy distribution characteristics of different stages.

As can be seen in Figure 4(a), the energy absorbed in the prepeak stage was mainly converted to elastic strain energy, accounting for about 72%~80% of the total energy, while dissipated energy remained 18% to 20%. As confining pressure increased, the amount of the stored elastic strain energy became larger. The elastic strain energy was $464 \text{ kJ}\cdot\text{m}^{-3}$ when confining pressure was 5 MPa, and when the confining pressure increased to 20 MPa, the elastic strain energy was $1102.6 \text{ kJ}\cdot\text{m}^{-3}$, with an apparent confining pressure effect. At this stage, the elastic strain energy generated by rock specimen's deformation can be continuously stored, while energy is consumed for the closure of cracks inside the rock specimens and the initiation and propagation of microcracks. As can be seen From Figure 4(b), the vast majority of the energy absorbed in the postpeak stage was transferred to dissipated energy, accounting for about 87% of the total energy. As the confining pressure increased, dissipated energy also increased. When confining pressure was 5 MPa, dissipated energy was $787 \text{ kJ}\cdot\text{m}^{-3}$. When confining pressure

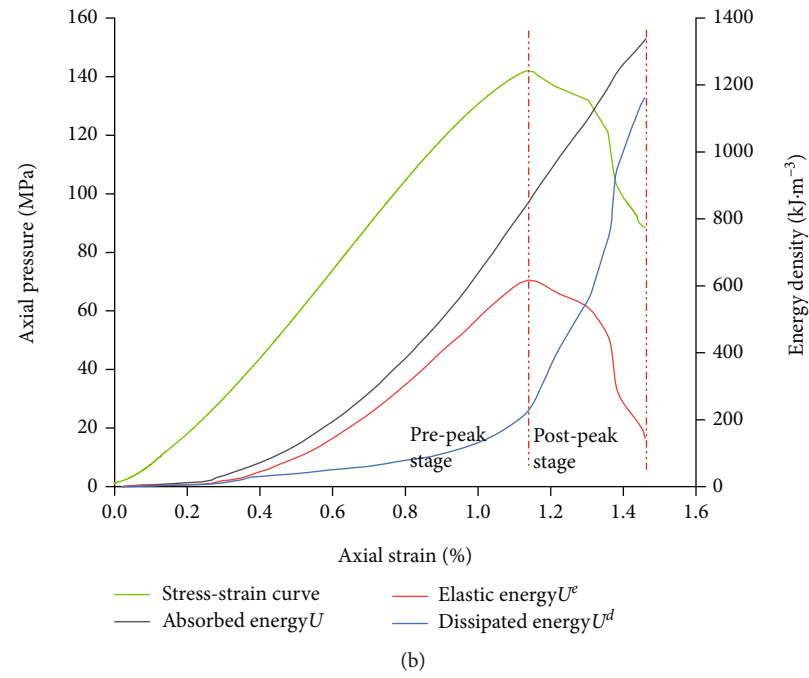
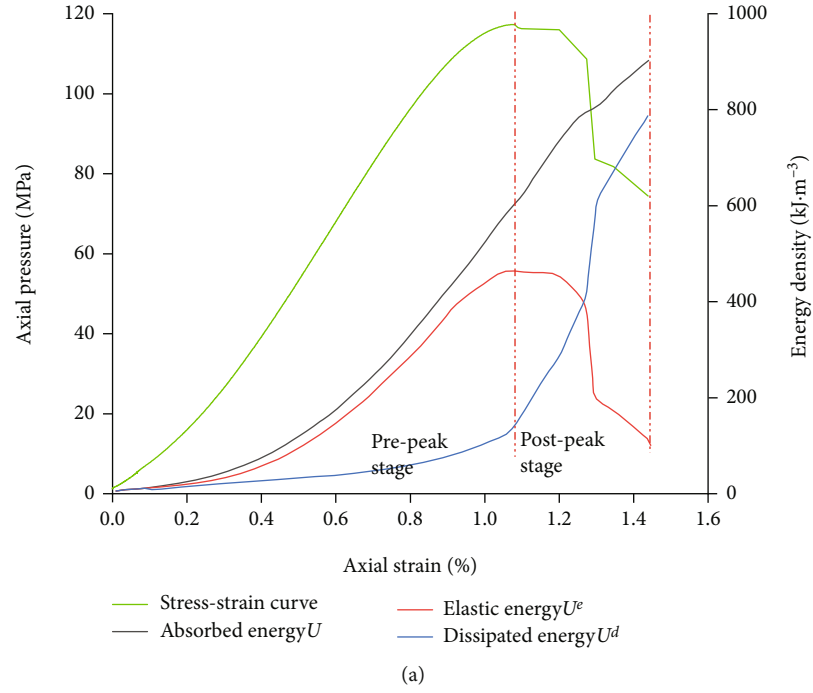


FIGURE 3: Continued.

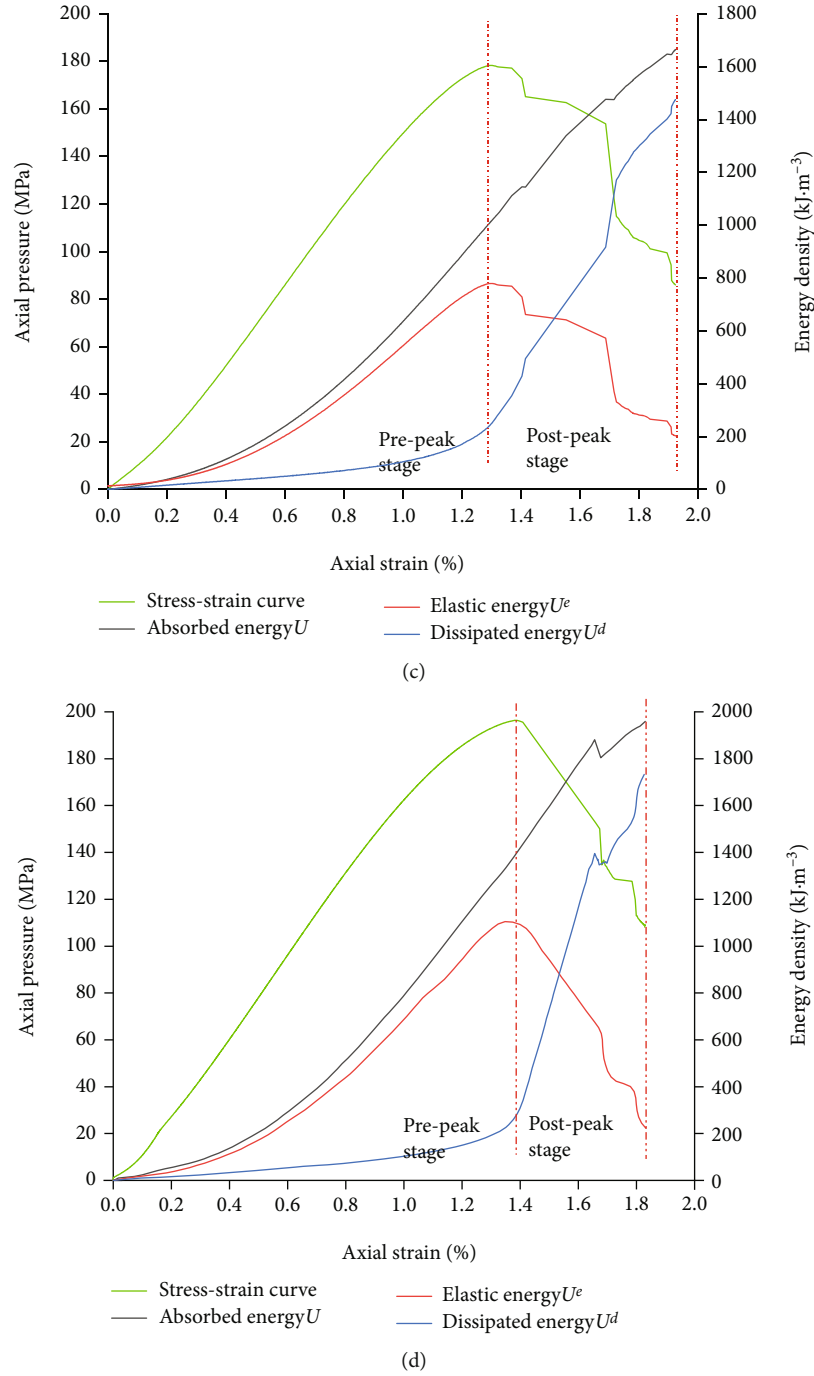


FIGURE 3: Energy evolution curve of sandstone under different confining pressure. (a) Confining pressure 5 MPa. (b) Confining pressure 10 MPa. (c) Confining pressure 15 MPa. (d) Confining pressure 20 MPa.

increased to 20 MPa, elastic strain energy was $1733 \text{ kJ} \cdot \text{m}^{-3}$. Elastic strain energy only accounted for a very small proportion. In this stage, a large number of macroscopic cracks form in the rock specimens and the total energy is mainly used for the formation and penetration of the macroscopic cracks. However, due to the existence of confining pressure, the rock specimens have certain residual strength, so a small amount of elastic strain energy can still be stored.

3. Energy Transformation of Roadway Surrounding Rock Numerical Simulation Method and Its Implementation

3.1. Energy Model of Roadway Surrounding Rock. Figure 5 shows the mechanical model diagram of the roadway surrounding rock. Figure 5(a) is the schematic diagram of the roadway excavation, Q_1 represents the underground space; Q_2 represents roadway surrounding rock; and Q_3 is

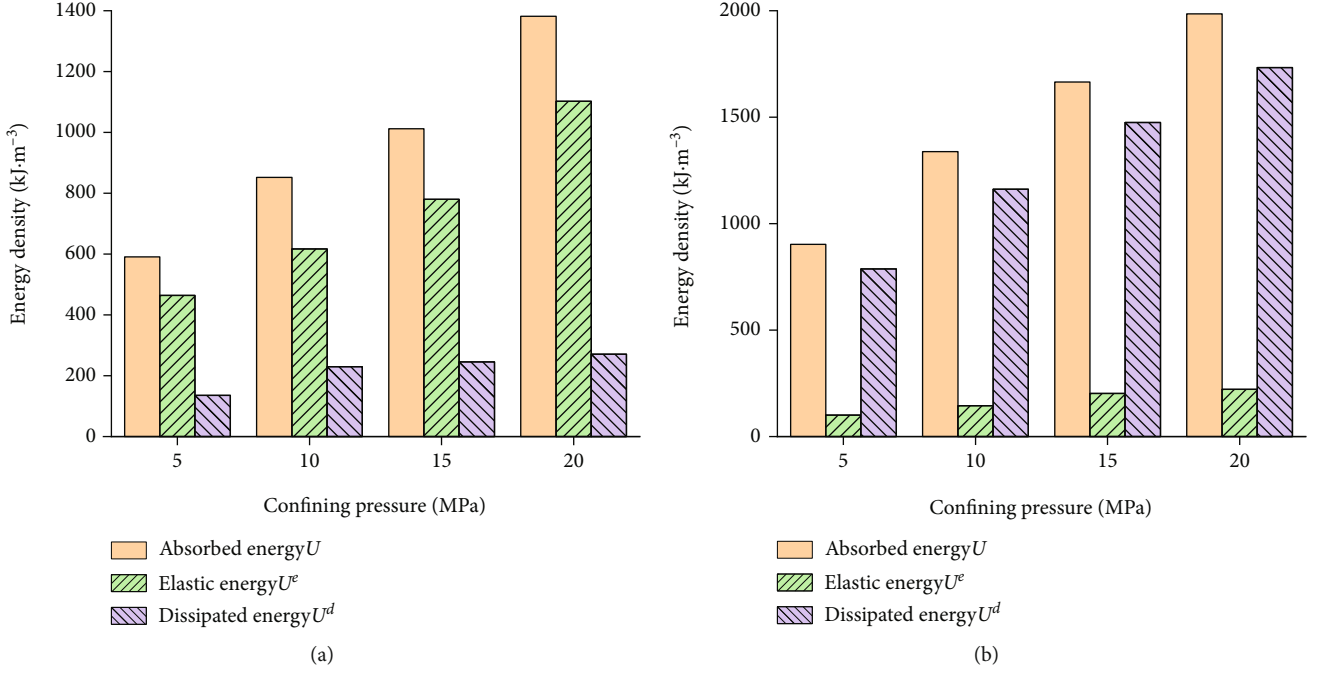


FIGURE 4: Energy distribution characteristics at different stages. (a) Prepeak stage. (b) Postpeak stage.

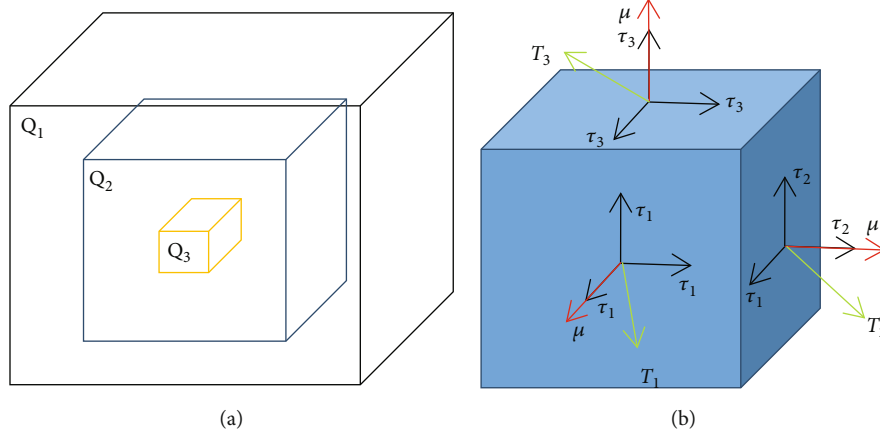


FIGURE 5: Mechanical model of roadway surrounding rock. (a) Schematic diagram of roadway surrounding rock. (b) The stress state of any point of surrounding rock.

roadway. The stress state of arbitrary point of surrounding rock is shown in Figure 5(b), which is represented by the stress component of the three orthogonal faces of the unit body. T_i indicates the stress component on arbitrary side. τ_{ij} is the stress state of the surface, μ_j is the normal unit vector of the surface, and the relationships among the three satisfies $T_i = \mu_j \tau_{ij}$ ($i, j = 1, 2, 3$).

Supposing the stable state before the roadway excavation is State I, and the stable state of the roadway surrounding rock after the stress adjustment is State II. The energy transformation process of roadway surrounding rock from State I to State II is shown in Figure 6. Energy input consists of two parts. One part is the work done by underground space Q_1 on surrounding rock Q_2 , which is called

the external force work. The other part is the work done by physical strength in the unit body of surrounding rock Q_2 , which is called internal work. Energy accumulation consists of elastic strain energy, and the main source is the difference between the elastic strain energy before and after the excavation, namely, the difference between U_I and U_{II} . Energy dissipation consists of two parts. The first part is elastic strain energy U_m stored in the excavated part of roadway surrounding rock Q_2 and the second part is the plastic energy generated by the plastic deformation of surrounding rock.

3.2. The Energy Model in $FLAC^{3D}$. In $FLAC^{3D}$ the elastic strain energy and the dissipated plastic energy of the

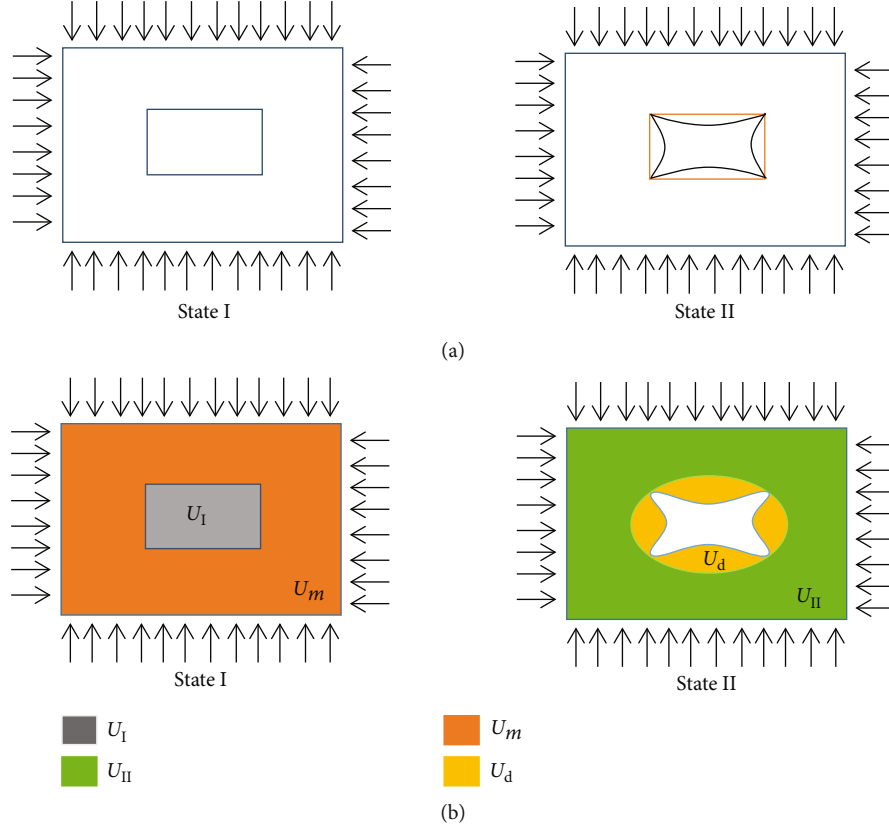


FIGURE 6: Schematic diagram of surrounding rock energy evolution. (a) Schematic diagram of energy input. (b) Schematic diagram of energy accumulation and dissipation.

unit body containing mechanical model can be calculated. The whole process is solved incrementally: the motion equation of grid points and the stress strain of the region are solved in each time step. In the process where the system reaches equilibrium, the increment of the energy component can be determined by the stress-strain equation [31–33]. Elastic strain energy W_e of the unit body can be expressed as

$$W_e = \frac{V}{2} \left(\frac{\sigma_{ij}^d \sigma_{ij}^d}{2G} + \frac{\bar{\sigma}}{K} \right), \quad (3)$$

where V is volume, σ_{ij} is partial stress, $\bar{\sigma}$ is mean stress, and G and K are bulk modulus and shear modulus, respectively.

Elastic strain energy increment ΔW_e is the difference between the elastic energy in successive time steps, which can be divided into shear elastic energy increment ΔW_{es} and volume elastic energy increment ΔW_{ev} . The expression is as follows:

$$\Delta W_e = W_e' - W_e = \Delta W_{es} + \Delta W_{ev}. \quad (4)$$

Total shear strain energy increment ΔW_{Ts} and total volume strain energy increment ΔW_{Tv} can be obtained through average stress, respectively

$$\Delta W_{Ts} = \frac{V}{2} \left[(\sigma_{ii} + \sigma'_{ii}) e_{ii} + 2(\sigma_{ij} + \sigma'_{ij}) e_{ij} \right], \quad (5)$$

$$\Delta W_{Tv} = \frac{3V}{2} (\bar{\sigma} + \bar{\sigma}') \bar{e}.$$

Plastic strain energy increment ΔW_p can be divided into shear plastic energy increment ΔW_{ps} and volume plastic energy increment ΔW_{pv} , which is the difference between total strain energy and elastic strain energy. The expression is shown as follows:

$$\Delta W_p = \Delta W_{ps} + \Delta W_{pv} = (\Delta W_{Ts} - \Delta W_{es}) + (\Delta W_{Tv} - \Delta W_{ev}). \quad (6)$$

The above energy formula is edited and transferred in the fish language built in FLAC^{3D} so as to obtain such energy evolution characteristics of roadway surrounding rock as elastic strain energy and plastic strain energy.

3.3. Case of Study. Take the left fourth coal ventilation roadway in the 93rd coal of Xinjian coal mine as an example. A

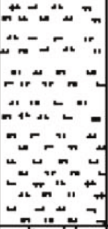


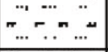
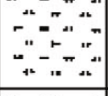

Title	Cohmnar	Thickness	Lithologic description
Medium sandstone		8.50	Offwhite, locally broken with coal dust
Siltstone-fire sandstone interbedding		8.00	Gray-light gray, with carcarbonized plantiennants
93 Coal		0.50	Black, mainly bright coal, block
Mid-fine sandstone		2.50	Gray-offwhite, locally taupe
Medium sandstone		3.50	Offwhite, containing coal dust, locally containing thin layer of coarse sandstone
Fine sandstone		7.00	Light gary, coarse containing thin layer of calcite and siltstone

FIGURE 7: Histogram of coal strata.

calculation model is established. In order to ensure the accuracy of the model, the stratigraphic parameters are appropriately simplified. The histogram of each stratum is shown in Figure 7. The left fourth coal ventilation roadway is a rectangular roadway which is 3 m in width and 2 m in height. The dimensions of the model are

$x \times y \times z = 35 \text{ m} \times 20 \text{ m} \times 30 \text{ m}$. The x -axis direction is trend, the y -axis direction is inclination, and the z -axis direction is gravity. There are 57576 nodes and 52400 unit bodies.

The constitutive relationship of the model adopts Mohr-Coulomb criterion. Displacement constraints are made on the four sides and bottom surface of the model. According to the stress test report and other data, $\sigma_z = 10.34 \text{ MPa}$ and $\sigma_x = 12.36 \text{ MPa}$ are applied to the model. Model schematic and boundary conditions is shown in Figure 8. The mechanical parameters of surrounding rock are shown in Table 1.

Figure 9 shows the nephogram of the distribution of the rock plastic zone of roadway surrounding rock. The shear failure of the two ribs and the top and bottom corner of the roadway appeared in different degrees and distributed roughly symmetrically. Compared with top corners, the destroyed range on bottom corners was larger. That is because the stress on the two ribs of roadway is transferred to the bottom corners, causing worse shear damage to bottom corners.

In the process of roadway excavation, the initial stress state of surrounding rock changes and the energy also

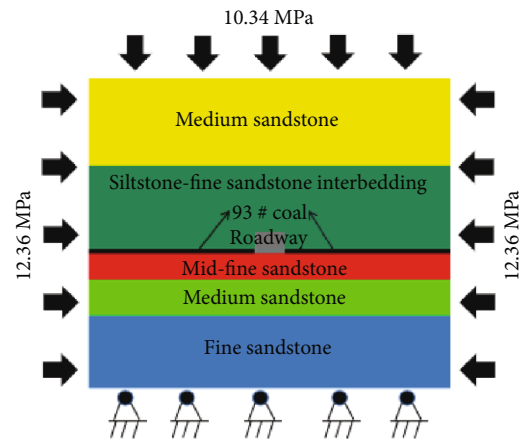


FIGURE 8: Model schematic and boundary conditions.

changes accordingly. Figure 10 is energy distribution nephogram of surrounding rock. As can be seen from Figure 10(a), the elastic strain energy of surrounding rock spreaded around the boundary of roadway. The spread range on the roof and floor was longer, which was roughly in the shape of strip with round ends. Both of ribs spreaded roughly in a circular way. The maximum of elastic strain energy density was $68.5 \text{ kJ} \cdot \text{m}^{-3}$, located in the position 1.2 m away from the two ribs of the roadway. As can be seen in Figure 10(b), the distribution range of plastic strain energy was consistent

TABLE 1: Mechanical parameters of surrounding rock.

Rock formation	Bulk modulus/GPa	Shear modulus/GPa	Cohesion/MPa	Internal frictional angle/°	Tensile strength/MPa	Density/kg·m ⁻³
Medium sandstone	7.2	5.4	4.46	32	3.09	2568
Siltstone-fine sandstone interbedding	8.5	6.3	3.54	31	3.03	2640
93# coal	5.3	3.1	2.36	28	1.68	1395
Midfine sandstone	10.3	7.8	3.25	32	2.62	2608
Medium sandstone	9.5	7.3	3.89	30	4.20	2568
Fine sandstone	9.8	6.2	4.02	32	2.89	2614

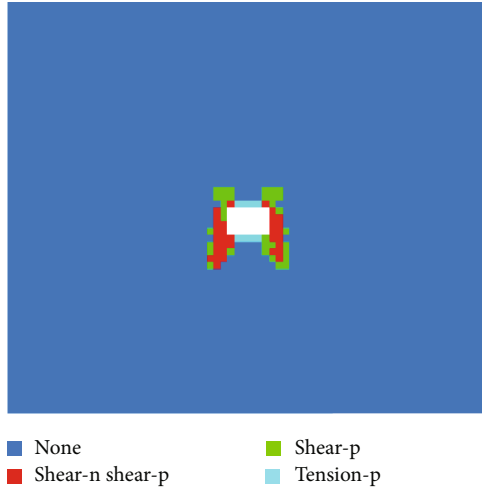


FIGURE 9: Plastic distribution nephogram of surrounding rock.

with plastic failure area, mainly distributing on the two ribs of the roadway, in the shape of semicircle, with a slightly larger bottom corners. Plastic strain energy spreaded from the both of ribs of the roadway. The spread range was about 1.2 m. The maximum of plastic strain energy density was $15.2 \text{ kJ} \cdot \text{m}^{-3}$, located in the boundary position of the two ribs. In fact, energy distribution of the roadway surrounding rock corresponds to plastic zone, which arises after surrounding rock reaches the yield state. This shows that, under those geological conditions, two ribs are the main sources of energy accumulation and dissipation.

Figure 11 shows energy characteristic change curve of the roadway ribs. The elastic strain energy density located within 1.2 m from the roadway surface was in the increase stage, rapidly increasing from $16.6 \text{ kJ} \cdot \text{m}^{-3}$ to $68.6 \text{ kJ} \cdot \text{m}^{-3}$. As the distance from the two ribs increased, elastic strain energy density decreased rapidly. When the distance increased to 6 m, the trend became stable gradually. Within the range 1.2 m from the surface of the roadway, plastic strain energy density decreased rapidly from $15.1 \text{ kJ} \cdot \text{m}^{-3}$ to about zero. That is because plastic deformation of the roadway arises on the two ribs. The range of plastic zone was roughly 1.2 m from the roadway surface. Plastic deformation of the roadway arose in this area, generating larger elastic strain energy and plastic strain energy. The deformation of sur-

rounding rock outside the plastic zone decreased gradually and the elastic strain energy decreased gradually while the plastic strain energy was zero.

4. Roadway Surrounding Rock Control Technology Based on Energy Transformation

Roadway is in a stable state before excavation, while stress distribution of roadway is adjusted after excavation. Stress concentration may occur in some positions, where a lot of energy may accumulate. According to the energy balance law [34–36], the accumulated energy is released substantially; plastic failure may arise in surrounding rock. The energy in this process is irreversible. The internal energy conversion of the fully elastic rock mass can be expressed as

$$W_c + U_m = U_c + W_r, \quad (7)$$

where W_c is the work done on rock mass by roadway excavation stress. U_m is the strain energy generated from the excavated rock mass; U_c is the strain energy accumulated for roadway excavation; and W_c is the elastic energy released by roadway excavation.

In the incompletely elastic roadway, W_r is approximate constant and U_m and U_c are fixed values, which are related to the geological conditions of roadway surrounding rock. Therefore, the internal energy transformation of incompletely elastic rock mass can be expressed as

$$U_m = U_c + W_r + W_n + W_f, \quad (8)$$

where U_c is the strain energy accumulated by the incompletely elastic roadway excavation, W_n is the energy released when the roadway is damaged and W_f is the energy absorbed by the support.

Based on the energy characteristics and rock energy evolution process, the control technology principle of roadway surrounding rock stability is proposed, as is shown in Figure 12. The first is reducing the elastic strain energy of surrounding rock. (1) By increasing the extension amount of the support. Part of the roadway energy is transferred to the support body, thus improving the energy release of surrounding rock; (2) By optimizing the layout of the roadway. Select the positions with good geological conditions for roadway construction, try to avoid the areas with such stress

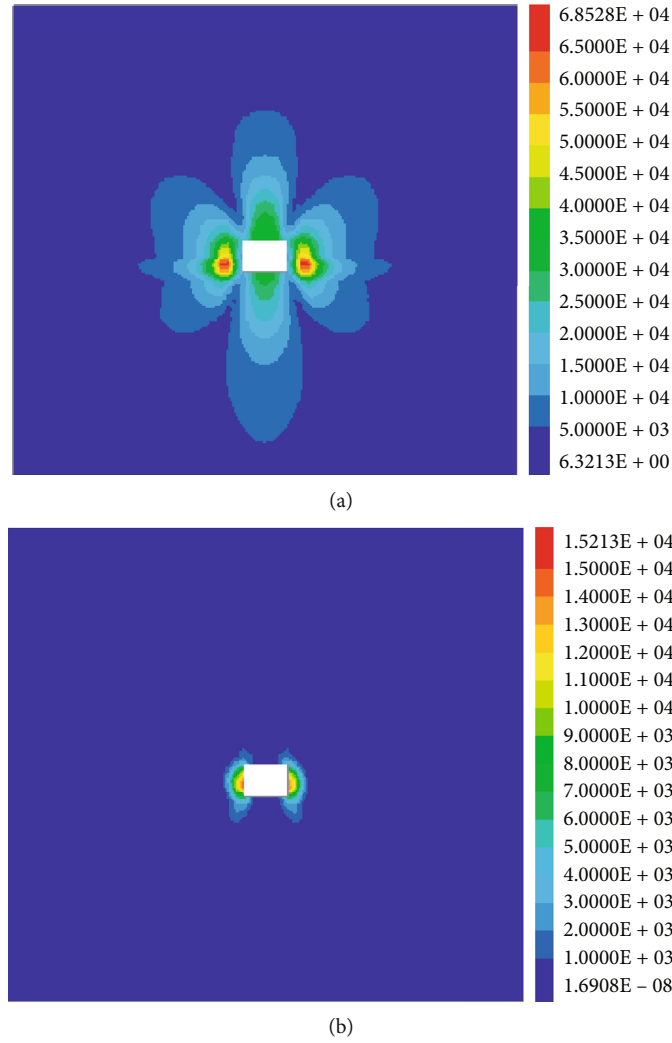


FIGURE 10: Energy density nephogram of roadway surrounding rock. (a) Elastic strain energy. (b) Plastic strain energy.

concentration as faults and geological structures to avoid stress concentration, thus reducing the energy accumulation of surrounding rock. The second is increasing the plastic strain energy of surrounding rock by setting weak structures, such as borehole pressure relief and other measures, to consume part of the energy in the coal body, thus improving the energy dissipation of surrounding rock.

5. Industrial Tests

5.1. Project Overview. The strike length of the right second working surface of the 91st coal of Xinjian coal mine is 800 m in depth, and the average dip length is 130 m. The average thickness of the coal seam is 1.4 m and the mean obliquity is 11° . Obliquity changes less and it tends to become larger from the east to the west. The occurrence of coal seam is stable and the coal type is 1/3 coking coal, which has stable structure and clear layer structure. The roof and floor is sandstone, which is gray and has high hardness.

The cross section of the transport roadway is trapezoidal, 4.0 m wide and the central axis height of 3.2 m. Joint anchor bolt-cable support is adopted. The anchor cable is 5.0 m long, the diameter is 17.8 mm and the row spacing is $2.0 \text{ m} \times 1.2 \text{ m}$. The bolt is 2.4 m long, with a 20.0 mm diameter and $1.0 \text{ m} \times 1.2 \text{ m}$ row spacing. The section support diagram is shown in Figure 13.

5.2. Stability Control Scheme of Roadway Surrounding Rock.

In the actual roadway engineering, the optimization of roadway layout is greatly limited by the geological conditions and excavation influence, which is only applicable to the initial stage of roadway construction. It is difficult to set weak structures for construction, which has high requirements for the size, height, and angle of weak structures. The energy release in roadway surrounding rock is mostly released in the form of deformation energy. For the roadway with specific geological conditions, the total amount of released energy is certain. Energy can be released on the support to reduce the energy amount on surrounding rock. Therefore,

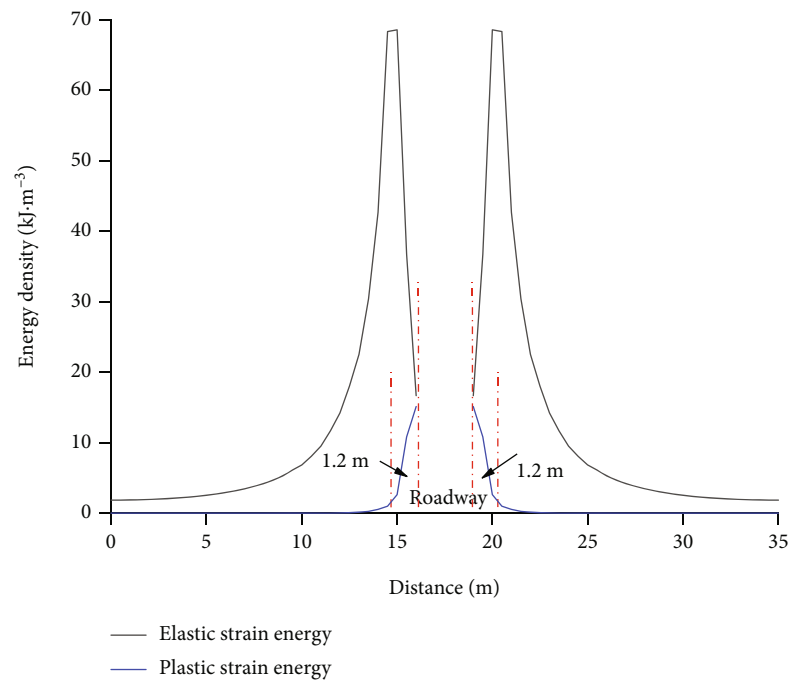


FIGURE 11: Energy change curve of ribs of roadway.

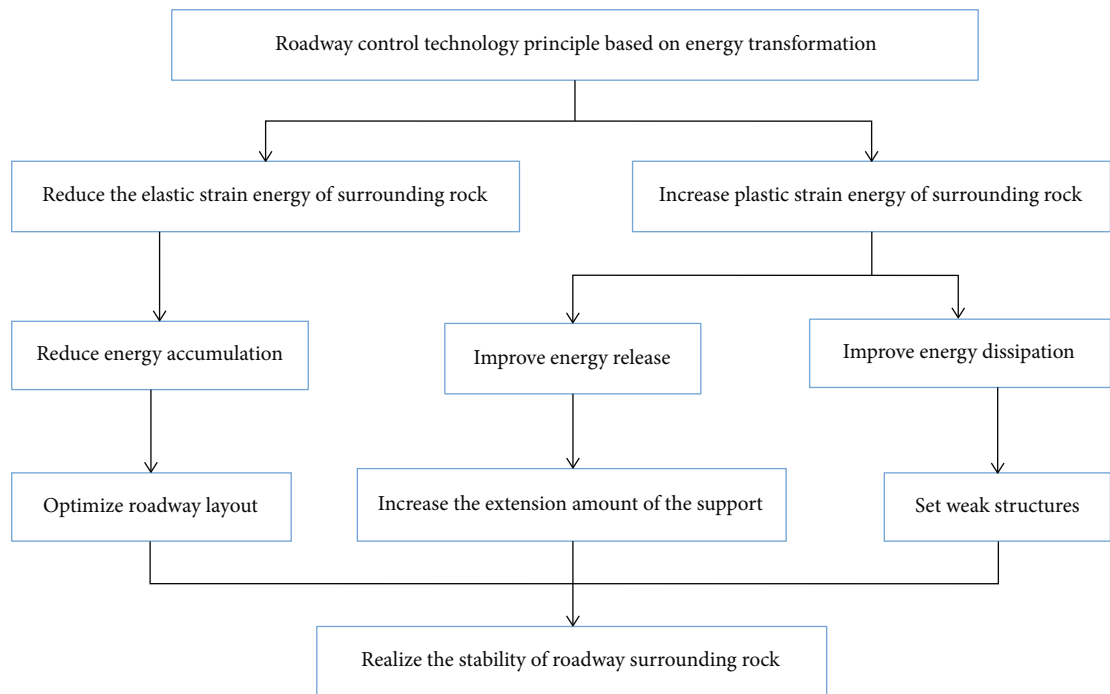


FIGURE 12: Roadway control technology principle based on the energy transformation.

roadway stability control is conducted mainly in terms of improving the energy release of surrounding rock.

5.2.1. Roadway Support Measures. (1) Control roof stability with high-density long anchor cable. On the basis of the original support, adjust the parameters of the support,

strengthen the supporting role of the anchor cable, and improve the integrity of surrounding rock so that the surrounding rock and the support body can form a complete bearing structure. Adopt high density long anchor cable, 7300 mm long, with a diameter of 21.8 mm, whose row spacing is 1000 mm × 1000 mm, arranged alternatively with

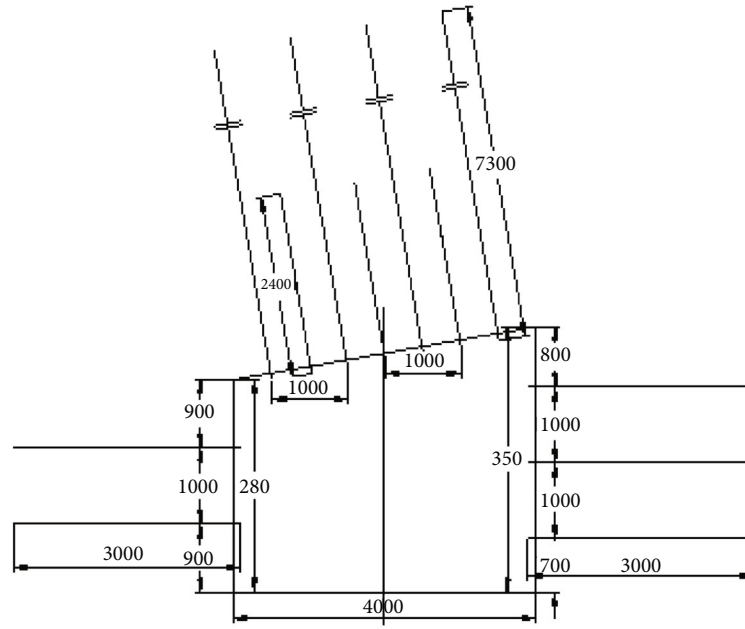


FIGURE 14: Optimized roadway section support map.

TABLE 2: Mechanical parameters and thickness of surrounding rock.

Rock formation	Bulk modulus/GPa	Shear modulus/GPa	Cohesion/MPa	Internal frictional angle/°	Tensile strength/MPa	Density/kg·m ⁻³	Thickness/m
Fine sandstone4	17.2	10.4	4.46	32	2.18	2568	2.35
Siltite2	18.5	11.3	3.54	31	2.35	2640	1.09
Middle sandstone3	19.8	12.1	2.36	28	1.98	1395	4.55
Fine sandstone3	10.3	9.8	3.25	32	2.62	2608	3.2
Siltite1	19.5	11.3	3.89	30	3.20	2568	1.38
91Coal	7.4	3.5	2.38	25	1.68	1398	1.35
Middle sandstone 2	19.8	12.1	2.36	28	1.98	1395	1.56
Fine sandstone 2	10.5	9.5	3.25	32	2.62	2608	2.2
90 coal	7.3	3.4	2.19	26	1.52	1396	0.85
Middle sandstone 1	19.8	12.1	2.36	28	1.98	1395	1.0
Fine sandstone 1	10.2	9.3	3.25	32	2.62	2608	5.95

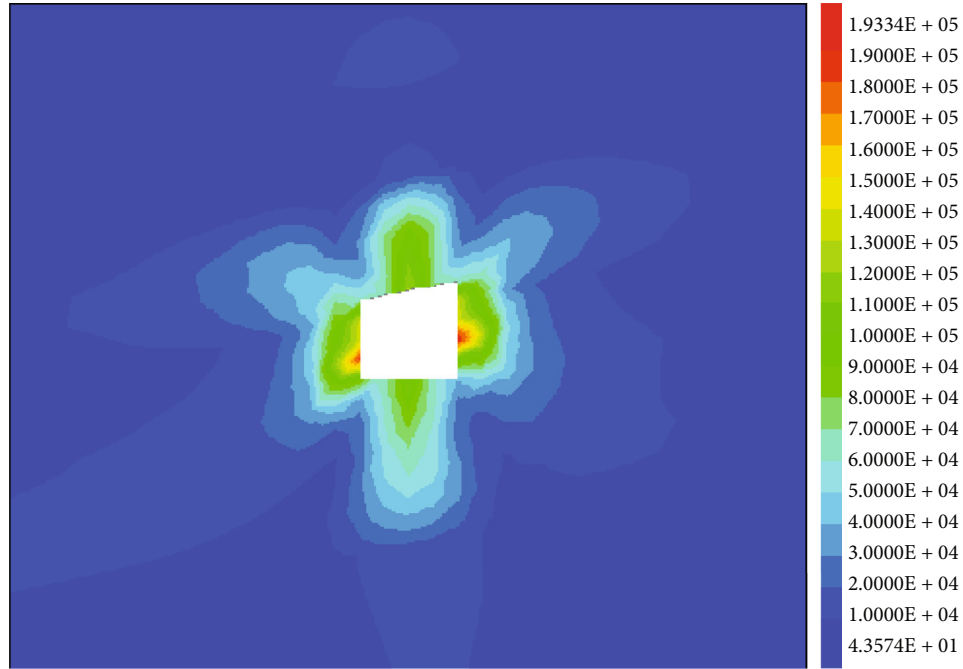
had a growth trend. The maximum of roof subsidence, floor heave and shrinkage of the right rib were 247 mm, 120 mm, and 292 mm, respectively. After the optimization, the increase rate of roadway surface displacement became slow on the whole, and the effect of floor was particularly obvious, which gradually became stable after 45 days. Each displacement amount decreased apparently: roof subsidence decreased to 62 mm, floor heave dropped to 26 mm, and right rib shrinkage dropped to 94 mm.

6. Discussion

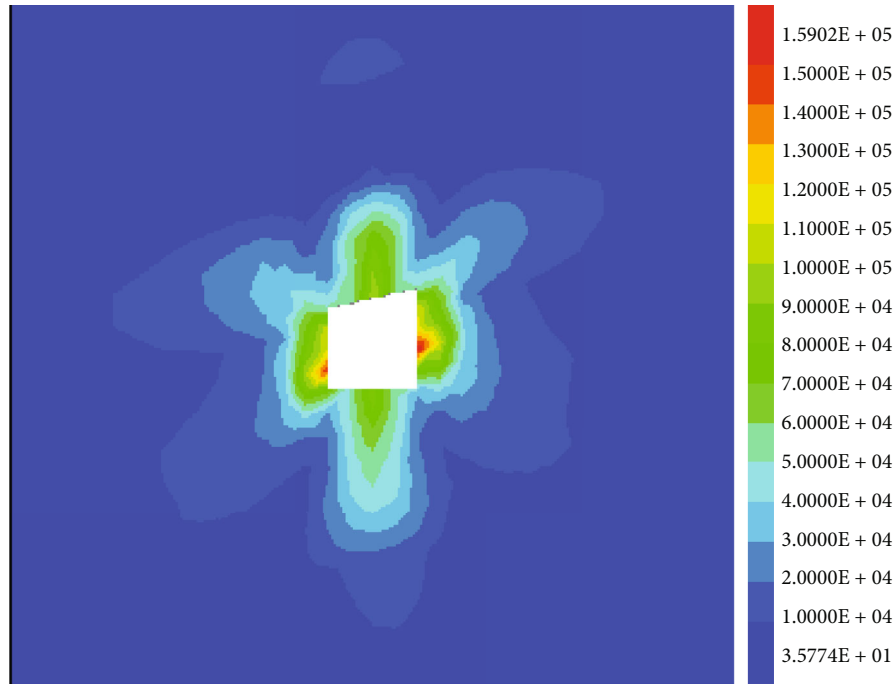
In this paper, based on elastic strain energy and plastic strain energy, the evolution law of sandstone energy characteristics and roadway surrounding rock energy evolution law were

obtained, respectively, through laboratory test and numerical simulation, and the stability control technology principle of roadway surrounding rock based on energy transformation is proposed. According to the geological conditions, the stability control of roadway surrounding rock was carried out. It shows that the technique principle is suitable for surrounding rock stability control, and the technique of surrounding rock stability control is a supplement to mechanics from the perspective of energy, and has a good application prospect.

In the process of rock deformation and failure under external force, the energy changes all the time. In this paper, the energy evolution law of rock specimens in the process of failure is studied by elastic strain energy and dissipation energy, ignoring energy characteristic parameters such as



(a)



(b)

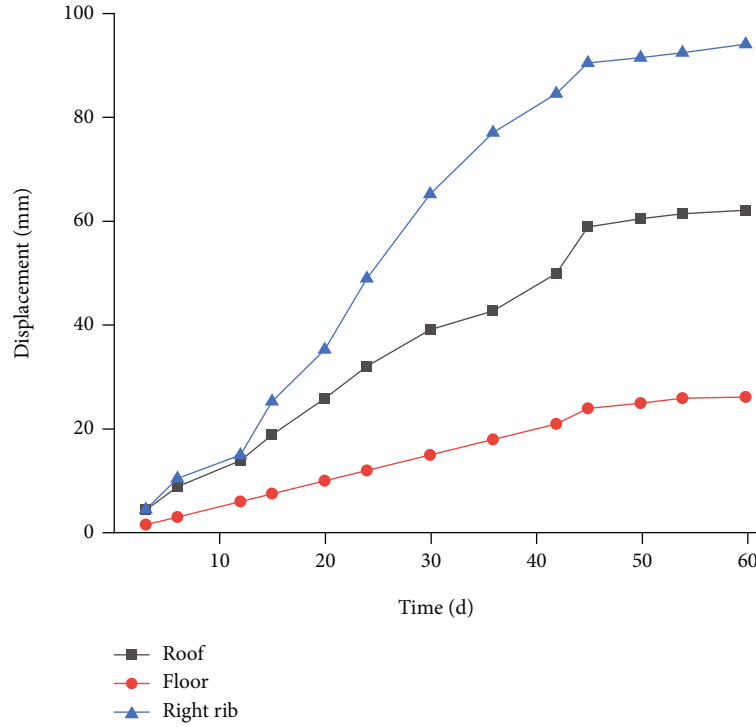
FIGURE 15: Elastic strain energy nephogram before and after optimization. (a) Original support. (b) After optimization.

frictional dissipation energy used between cracks in the process of energy evolution, thus there are some errors in the description of energy evolution in the whole process of deformation and failure.

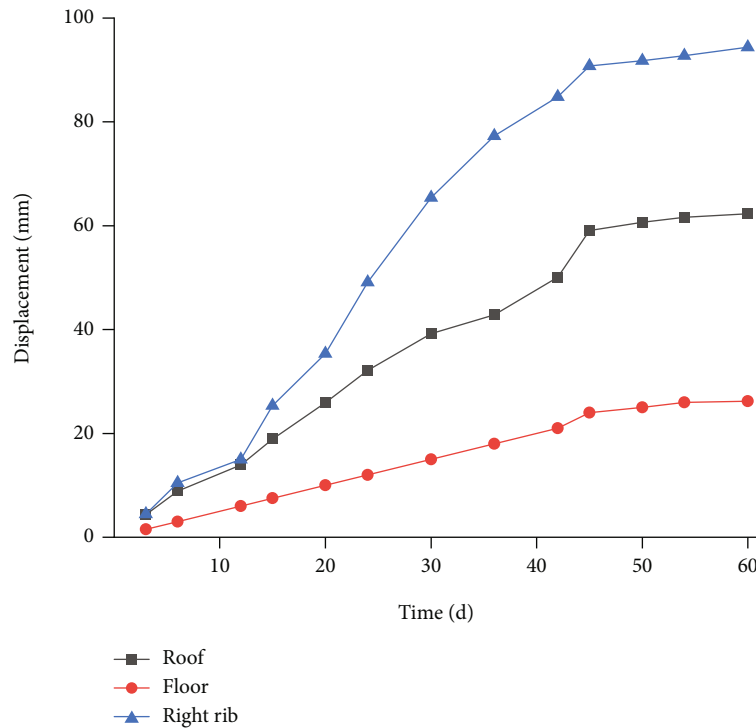
The stability of roadway surrounding rock can be reflected by the energy transformation of surrounding rock. The numerical model of roadway surrounding rock energy established in this paper is based on the elastic strain energy and plastic strain energy of surrounding

rock, which has good application effect, but lacks the verification of field application. Therefore, the energy of roadway surrounding rock can be quantified by combining seismological principle.

From the perspective of energy transformation, the principle of roadway surrounding rock stability control technology is put forward. Due to the limitation of geological conditions, this paper only carried out field construction aiming at improving the energy release principle of



(a)



(b)

FIGURE 16: Surface displacement curve of roadway. (a) Before the optimization. (b) After the optimization.

surrounding rock, and achieved good application effect. The effect of improving the energy dissipation of surrounding rock, reducing the energy accumulation, and the synergistic effect of each other have not been verified in the field, so corresponding research should be carried out.

7. Conclusion

In this paper, based on the research of the energy evolution regularity of sandstone samples, the surrounding rock energy numerical model was established, and then the

principle of roadway surrounding rock stability control technology is put forward. Field industrial test results show that the control effect is good. The main conclusions are as follows:

- (1) In the process of rock deformation and failure, the total energy increased exponentially before the axial stress peak, mainly transferred to elastic strain energy, accounting for about 72%~80% of the total energy and the dissipated energy remained 18%~20%. The total energy growth rate decreased slightly in the postpeak stage. The vast majority of energy was transferred to dissipated energy, accounting for about 87% of the total energy
- (2) Combined with energy transformation, put forward the principle of roadway surrounding rock stability control technology: one is to reduce the elastic strain energy of surrounding rock. On the one hand, by increasing the extension amount of support body, part of roadway energy is transferred to support body, thus improving the energy release of surrounding rock. On the other hand, by optimizing roadway layout, stress concentration is avoided and energy accumulation of surrounding rock is reduced. The second is to increase the plastic strain energy of surrounding rock, that is, to increase the energy dissipation of surrounding rock by setting weak structure
- (3) After the optimization of support measures, the roadway surface displacement and its increase rate decreased significantly, roof subsidence decreased from 247 mm to 62 mm, floor heave decreased from 120 mm to 26 mm, and the right rib shrinkage decreased from 292 mm to 94 mm, that is, the floor heave control effect was particularly obvious. The deformation of surrounding rock gradually stabilized after 45 days

Data Availability

The data used to support the study is available within the article.

Conflicts of Interest

The authors declare that they have no conflicts of interest.

Acknowledgments

This study was supported by the National Natural Science Foundation of China (51774122), Outstanding Young Talents Project supported by the Central Government for The Reform and Development of Local Universities (2020YQ13), and the Natural Science Foundation of Heilongjiang Province (LH2019E087).

References

- [1] Q. L. Zou, H. Liu, Z. H. Cheng, T. C. Zhang, and B. Q. Lin, "Effect of slot inclination angle and borehole-slot ratio on mechanical property of pre-cracked coal: implications for ECBM recovery using hydraulic slotting," *Natural Resources Research*, vol. 29, no. 3, pp. 1705–1729, 2020.
- [2] X. L. Li, Z. H. Li, E. Y. Wang et al., "Pattern recognition of mine microseismic and blasting events based on wave fractal features," *Fractals*, vol. 26, no. 3, article 1850029, 2018.
- [3] X. L. Li, Z. Y. Cao, and Y. L. Xu, "Characteristics and trends of coal mine safety development," *Energy Sources, Part A: Recovery, Utilization, and Environmental Effects*, vol. 11, pp. 1–9, 2020.
- [4] H. P. Kang, P. F. Jiang, B. X. Huang et al., "Roadway strata control technology by means of bolting-modification-destressing in synergy in 1000 m deep coal mines," *Journal of China Coal Society*, vol. 45, no. 3, pp. 845–864, 2020.
- [5] W. J. Wang, C. Yuan, W. J. Yu et al., "Stability control method of surrounding rock in deep roadway with large deformation," *Journal of China Coal Society*, vol. 41, no. 12, pp. 2921–2931, 2016.
- [6] X. X. Chen and J. P. Wu, "Study on the mechanism and control technology of large deformation of roadway surrounding rock in the fault fracture zone," *Journal of Mining & Safety Engineering*, vol. 35, no. 5, pp. 885–892, 2018.
- [7] P. Peng, D. L. Zhang, and Z. Y. Sun, "Deformation characteristics of surrounding rock and reinforcement parameter design of weak interlayer tunnels," *Chinese Journal of Rock Mechanics and Engineering*, vol. 40, no. 11, pp. 2260–2272, 2021.
- [8] H. S. Jia, K. Pan, D. F. Li et al., "Roof fall mechanism and control method of roof with weak interlayer in mining roadway," *Journal of China University of Mining & Technology*, vol. 51, no. 1, pp. 67–76, 2022.
- [9] H. P. Xie, R. D. Peng, and Y. Jv, "Energy dissipation of rock deformation and fracture," *Chinese Journal of Rock Mechanics and Engineering*, vol. 23, no. 21, pp. 3565–3570, 2004.
- [10] H. P. Xie, R. D. Peng, Y. Jv, and H. W. Zhou, "Preliminary study on energy analysis of rock failure," *Chinese Journal of Rock Mechanics and Engineering*, vol. 24, no. 15, pp. 2603–2608, 2005.
- [11] H. P. Xie, Y. Jv, and L. Y. Li, "Criteria for strength and structural failure of rocks based on energy dissipation and energy release principles," *Chinese Journal of Rock Mechanics and Engineering*, vol. 24, no. 17, pp. 3003–3010, 2005.
- [12] J. Xu, Y. Zhang, H. W. Yang, and J. N. Wang, "Energy evolution law of deformation and damage of sandstone under cyclic pore water pressures," *Chinese Journal of Rock Mechanics and Engineering*, vol. 30, no. 1, pp. 141–148, 2011.
- [13] G. Y. Zhao, B. Dai, L. J. Dong, and C. Yang, "Energy conversion of rocks in process of unloading confining pressure under different unloading paths," *Transactions of Nonferrous Metals Society of China*, vol. 25, no. 5, pp. 1626–1632, 2015.
- [14] X. B. Yang, H. M. Cheng, and Y. Y. Pei, "Study on the evolution characteristics of rock deformation and post-peak energy under different loading methods," *Chinese Journal of Rock Mechanics and Engineering*, vol. 39, no. S2, pp. 3229–3236, 2020.
- [15] Z. X. Liu, G. M. Zhao, X. R. Meng et al., "Analysis of creep energy evolution of red sandstone based on linear energy storage law," *Journal of Central South University (Science and Technology)*, vol. 52, no. 8, pp. 2748–2760, 2021.

- [16] Q. B. Meng, C. K. Wang, B. X. Huang et al., "Rock energy evolution and distribution law under triaxial cyclic loading and unloading conditions," *Chinese Journal of Rock Mechanics and Engineering*, vol. 39, no. 10, pp. 2047–2059, 2020.
- [17] Z. Hao, L. F. Guo, X. D. Zhao, G. X. Chen, and G. H. Zhang, "Analysis of burst failure energy characteristics of mining roadway surrounding rock," *Journal of China Coal Society*, vol. 45, no. 12, pp. 3995–4005, 2020.
- [18] H. Yu, X. J. Zhang, B. Y. Li, and F. J. Chu, "Macro-micro mechanical response and energy mechanism of surrounding rock under excavation disturbance," *Journal of China Coal Society*, vol. 45, no. S1, pp. 60–69, 2020.
- [19] H. Y. Shi, N. J. Ma, J. J. Shi, N. Li, and G. W. Tan, "Simulation study on energy evolution and release of surrounding rock in stope," *Coal Science and Technology*, vol. 48, no. 3, pp. 106–111, 2020.
- [20] S. W. Wang, W. J. Ju, J. F. Pan, and C. Lu, "Mechanism of energy partition evolution of excavation roadway rockburst in coal seam under tectonic stress field," *Journal of China Coal Society*, vol. 44, no. 7, pp. 2000–2010, 2019.
- [21] P. Huang, S. Spearing, F. Ju, K. V. Jessu, Z. W. Wang, and P. Ning, "Control effects of five common solid waste back filling materials on in situ strata of gob," *Energies*, vol. 12, no. 1, 2019.
- [22] Z. Q. Ma, C. M. Tao, Y. J. Zuo, G. Y. Wu, and P. Liu, "Supporting technology of roadways with thick and soft roof based on energy balance theory," *Journal of Mining and Safety Engineering*, vol. 35, no. 3, pp. 496–502, 2018.
- [23] R. D. Peng, Y. Jv, F. Gao, H. P. Xie, and P. Wang, "Energy analysis on damage of coal under cyclical triaxial loading and unloading conditions," *Journal of the China Coal Society*, vol. 39, no. 2, pp. 245–252, 2014.
- [24] S. Gao, L. M. Zhang, Z. Q. Wang, and Y. Cong, "Study of deformation and energy properties of marble unloading failure," *Chinese Journal of Rock Mechanics and Engineering*, vol. 33, no. S1, pp. 2808–2813, 2014.
- [25] T. Qin, Y. W. Duan, H. R. Sun, H. L. Liu, and L. Wang, "Energy evolution and acoustic emission characteristics of sandstone specimens under unloading confining pressure," *Shock and Vibration*, vol. 2019, Article ID 1612576, 9 pages, 2019.
- [26] X. J. Dong, A. Karrech, H. Basarir, M. Elchalakani, and A. Seibi, "Energy dissipation and storage in underground mining operations," *Rock Mechanics and Rock Engineering*, vol. 52, no. 1, pp. 229–245, 2019.
- [27] T. Qin, Y. W. Duan, H. R. Sun, L. Wang, and H. L. Liu, "Mechanical characteristics and energy dissipation characteristics of sandstone under triaxial stress conditions," *Journal of the China Coal Society*, vol. 45, no. S1, pp. 255–262, 2020.
- [28] Z. Z. Zhang and F. Gao, "Confining pressure effect on rock energy," *Chinese Journal of Rock Mechanics and Engineering*, vol. 34, no. 1, pp. 1–11, 2015.
- [29] Z. Y. Li, G. Wu, T. Z. Huang, and Y. Liu, "Variation of energy and criteria for strength failure of shale under triaxial cyclic loading," *Chinese Journal of Rock Mechanics and Engineering*, vol. 37, no. 3, pp. 662–670, 2018.
- [30] B. Dai, G. Y. Zhao, H. Konietzky, and P. L. P. Wasantha, "Experimental investigation on damage evolution behaviour of a granitic rock under loading and unloading," *Journal of Central South University*, vol. 25, no. 5, pp. 1213–1225, 2018.
- [31] J. Q. Guo, X. R. Liu, J. B. Wang, and Z. H. Huang, "Strength criterion of rock based on elastic strain energy," *Rock and Soil Mechanics*, vol. 37, no. S2, pp. 129–136, 2016.
- [32] Q. Sun, S. C. Li, X. D. Feng, W. T. Li, and C. Yuan, "Study of numerical simulation method of rock fracture based on strain energy density theory," *Rock and Soil Mechanics*, vol. 32, no. 5, pp. 1575–1582, 2011.
- [33] Itasca Consulting Group Inc, *FLAC3D 5.0 manual*, ICG, Minneapolis, 2010.
- [34] W. L. Gong, D. Y. Zhu, J. Wang, M. C. He, and D. L. Wang, "Deformation and energy equation verification of NPR anchor cable support roadway based on model test," *Journal of Mining and Safety Engineering*, vol. 37, no. 5, pp. 918–927, 2020.
- [35] G. Y. Cui, B. H. Song, M. N. Wang, D. Y. Wang, and X. G. Wu, "Study on the anti-breaking design method of tunnel across active fault based on the energy balance method," *China Civil Engineering Journal*, vol. 53, no. S2, pp. 309–314, 2020.
- [36] T. B. Zhou, Y. P. Qin, Q. F. Ma, and J. Liu, "A constitutive model for rock based on energy dissipation and transformation principles," *Arabian Journal of Geosciences*, vol. 12, no. 15, p. 492, 2019.